Numerical Modeling of Tip Vortex Flow of Marine Propellers

Sangwoo Pyo

Seoul National University, San 56-1, Shillim-dong, Kwanak-gu,Seoul, Korea

Abstract

The accurate prediction of the flow and the pressure distribution near the tip of the blade is crucial in determining the tip vortex cavitation inception which usually occurs on the blade tip or inside the core of the tip vortex just downstream of the blade tip. An improved boundary element method is applied to the prediction of the flow around propeller blades, with emphasis at the tip region. In the method, the flow adapted grid and a higher order panel method, which combines a hyperboloidal panel geometry with a bi-quadratic dipole distribution, are used in order to accurately model the trailing wake geometry and the highly rolled-up regions in the wake. The method is applied to several propeller geometries and the results have been found to agree well to the existing experimental data.

Inviscid flow methods are able to predict the pressures at the tip as well as the shape of the trailing wake. On the other hand, they are unable to determine the flow inside the viscous core of the tip vortex, where cavitation inception often occurs. Thus, a method is presented that treats the flow inside the viscous core. The inner flow is treated with a 2-D Navier-Stokes solution *without* making any assumptions for axisymmetric flow and conicity of the flow along the tip trajectory. The method can thus allow the treatment of general propeller blade configurations. The velocity and pressure distributions inside the core are shown and compared to those from other numerical methods.

1 Introduction

In most marine propeller applications cavitation usually occurs first in the strong vortical region in the vicinity of the blade tip. Inception at the tip may occur either on the blade or in the vortex core (downstream of the blade). Knowing the details of the flow on and/or behind the tip is thus *crucial* in determining cavitation inception. Tip vortex cavitation has been one of the loudest underwater noise sources. Due to this, tip vortex cavitation has been of great interest in naval propeller design. A tip vortex is most likely to cavitate when the blade tip is subject to off-design conditions, due to spatial non-uniformity of the inflow to the propeller, or due to flow inclination. In order to delay tip vortex cavitation inception, designers often unload the circulation distribution at the tip, thus by sacrificing on propeller efficiency. Therefore, in the design and assessment of propulsors for naval applications, it is essential to accurately predict and thus control tip vortex cavitation inception.

The primary methods for predicting tip vortex cavitation inception are variations of the method by McCormick [McCormick, 1962]. In the method, a semi-empirical approach is proposed in

which the minimum pressure is considered to depend on the near-tip loading and the tip boundary layer. Then a power law relation, $\delta \sim Re^{-r}$, between the boundary layer thickness δ and the local Reynolds number Re is suggested. The constant factor multiplying this scaling law as well as the exponent are geometry dependent and thus the method can provide predictions only for geometries which are close to those that have been tested in either model or full scale. Recently, from LDV measurements in the vicinity of the tip vortex for several planar wing configurations, at different tunnel facilities and flow conditions, it has been shown that the velocity field close to the core of the vortex depends on two parameters; (1) the strength of the tip vortex along its trajectory and (2) the radius of the vortex core [Fruman et al., 1992]. Having these parameters, the value of the minimum pressure inside the vortex core and its location along the vortex can be readily determined. The corresponding pressure coefficient should then be equal to the negative value of the cavitation number at inception. More Recently, Reynolds Averaged Navier-Stokes solvers are applied for the analysis of the tip vortex. An attempt by Dupont et al. shows poor predictions of the minimum pressure in the vortex core, mainly due to the overprediction of the size of the vortex viscous core [Dupont and Cerrutti, 1991]. Other attempts with the viscous flow method [Eça et al., 1994], [Stern et al., 1994], have not been able either to capture accurately the size of the core or the pressure distribution inside the core of a tip vortex.

On the other hand, panel methods have been found to be useful in determining the minimum pressure coefficient at the blade tip, which then can be correlated with the cavitation number at tip vortex cavitation inception [Pyo, 1995]. It is believed that a *robust* panel method, with full wake alignment , will not only improve the accuracy of the predicted pressure distributions at the blade tip, but also will provide the foundation for predicting the tip vortex evolution which will ultimately lead to more reliable estimates of tip vortex cavitation inception.

In the present paper, an improved boundary element method is applied to the prediction of the flow around the lifting surface, with emphasis at the tip region. In the method, the trailing wake geometry is essential in determining the forces on the lifting surface, especially at off-design conditions. A higher order panel method, which combines a hyperboloidal panel geometry [Hsin, 1990] with a bi-quadratic dipole distribution and the 06 Adapted Grid [Pyo, 1995], is used in order to accurately model the highly rolled-up regions. The method is applied to several propeller geometries and the results have been found to agree very well to the existing experimental data [Jessup, 1989]. In particular, the method has been found to capture the trace of the tip vortex very accurately and also determine the velocity flow field behind the lifting surfaces very well.

Inviscid flow methods are able to predict the pressures at the tip as well as the shape of the trailing wake [Pyo, 1995]. They are unable though of determining the flow inside the viscous core of the tip vortex, where cavitation inception often occurs. Thus, a viscous method is suggested for the analysis of the flow inside the viscous core. In the method, the flow is treated with a 2-D Navier-Stokes solution *without* making any assumptions for axisymmetric flow. The method can thus allow the treatment of general lifting surface configurations.

2　The flow outside the core

For $Re \to \infty$, the flow outside the core can be represented as an inviscid potential flow with wake sheet roll-up, also known as the ideal wake calculation. This flow is treated with a high order panel method in three dimensions [Pyo 1995].

2.1 Formulation

The flow is assumed to be inviscid, incompressible and irrotational everywhere, except in the thin wake sheet. The flow velocity can be written as a superposition of the incoming flow U_{in}, the velocities induced by the body, V_B, and by the wake sheet, V_W. The velocity vector, thus has the form

$$V = U_{in} + V_B + V_W = U_{in} + \nabla \phi$$

where ϕ is an induced potential due to the body and the wake.
In the fluid domain, the potential satisfies the Laplace equation

$$\nabla^2 \phi = 0. \tag{1}$$

Denoting the body surface as S_B, the kinematic boundary condition on S_B is

$$\nabla \phi \cdot n = -U_{in} \cdot n \tag{2}$$

where n is an unit normal vector on the body.
Applying the Green's theorem with the Laplace equation (1), the induced potential and velocity can be expressed by

$$\phi(p) = \frac{1}{4\pi} \int \int_{S_B} \left[\phi(q) \frac{\partial}{\partial n_q} \frac{1}{R(p;q)} - \frac{\partial \phi}{\partial n_q} \frac{1}{R(p;q)} \right] dS$$
$$+ \frac{1}{4\pi} \int \int_{S_W} \Delta\phi(q) \frac{\partial}{\partial n_q} \frac{1}{R(p;q)} dS \tag{3}$$

$$\nabla_p \phi(p) = \frac{1}{4\pi} \int \int_{S_B} \left[\phi(q) \frac{\partial}{\partial n_q} \nabla \frac{1}{R(p;q)} - \frac{\partial \phi}{\partial n_q} \nabla \frac{1}{R(p;q)} \right] dS$$
$$+ \frac{1}{4\pi} \int \int_{S_W} \Delta\phi(q) \frac{\partial}{\partial n_q} \nabla \frac{1}{R(p;q)} dS \tag{4}$$

where q is a source point and p is a field point which may be located anywhere in the space. S_W is the wake surface.

2.2 Numerical implementation

The propeller surface and the wake sheet are discretized into hyperboloidal panels [Hsin 1990]. Constant strength sources and dipoles are distributed on each panel on the body and bi-quadratic strength dipoles on each panel in the wake. The effect of the hub is also included by distributing panels on the hub surface. A collocation method is applied, with the control points being the centroids of the panels. Using equations (2) and (4), the discretized form of the induced velocity becomes :

$$\nabla \phi_i = \sum_{K=1}^{N_{BLADE}} \sum_{j=1}^{N_{PANEL}} a_{i,j}^K \phi_j^K - \sum_{K=1}^{N_{BLADE}} \sum_{j=1}^{N_{PANEL}} b_{i,j}^K \frac{\partial \phi_j^K}{\partial n}$$

21

$$+ \sum_{K=1}^{N_{BLADE}} \sum_{m=1}^{M} \sum_{l=1}^{N_W} W_{i,m,l}^{K}$$

$$a_{i,j} = \frac{1}{4\pi} \int \int_{S_j} \frac{\partial}{\partial n_j} \nabla \frac{1}{R_{i,j}} dS_j$$

$$b_{i,j} = \frac{1}{4\pi} \int \int_{S_j} \nabla \frac{1}{R_{i,j}} dS_j$$

$$W_{i,m,l} = \frac{1}{4\pi} \int \int_{S_{m,l}} (b_0 + b_1 \xi + b_2 \eta + b_3 \xi \eta + b_4 \xi^2 + b_5 \eta^2 + b_6 \xi \eta^2 +$$

$$b_7 \xi^2 \eta + b_8 \xi^2 \eta^2) \frac{\partial}{\partial n_{m,l}} \nabla \frac{1}{R_{i,m,l}} dS_{m,l} \qquad (5)$$

where N_{BLADE} is the number of blades and N_{PANEL} is the total number of panels on a blade and a hub, which has M spanwise panels on the blade. N_W is the number of streamwise panels on each strip in the wake. ξ and η are local coordinates on the panel surface.

The influence coefficients $a_{i,j}$ and $b_{i,j}$ are defined as the velocities induced at panel i by a unit strength dipole and source, respectively, located at panel j on blade K. The wake influence co-efficient $W_{i,m,l}^{K}$ is defined similarly, as the induced velocity at panel i due to the unit dipole at (m, l) in the wake on the blade K. The numerical computation of these coefficients is explained in [Maniar, 1995] and [Pyo, 1995].

In order to construct the 06 Adapted Grid including the effect of the wake sheet roll-up, the following procedure is implemented.

1. Solve the equation (3) with a geometry of the trailing wake sheet, which is aligned with the inflow. The strength of the source $(\frac{\partial \phi_j}{\partial n}^K)$ and the dipole (ϕ_j^K) on the body and the dipole $(\Delta \phi_{m,l}^K)$ in the wake are found [Lee, 1987], [Hsin, 1990].

2. Compute the induced velocities $(\nabla \phi_i)$ at the control points of the first row of panels in the wake from the equation (5). Then move the first row of panels to the second row by using a first order Euler scheme, which is given as,

$$x_{m,i+1} = x_{m,i} + (U_{in} + \nabla \phi_{m,i}) \cdot \frac{\Delta t_i}{2} \qquad (i = 1)$$

3. Adjust the downstream wake shape so that it has the same shape as the wake at the previous row. In other words, set $y_{k,j} = y_{i,j}$ and $z_{k,j} = z_{i,j}$ for $k = i + 1, i + 2, \cdots, N_{W+1}$, as shown in Figure 1. Also check the panel size. If the panel size is greater than the criterion Δ_{max}, then rediscretize the row in the spanwise direction.

4. Repeat steps 2. and 3. until the last row of the panels. With this initial geometry, compute induced velocities at all control points in the wake and move the panels all together. Repeat this calculation until the geometry of the wake sheet is converged. Usually, two iterations have been found to be enough.

5. With the converged wake sheet, construct the 06 Adapted Grid [Pyo, 1995] and solve the equation (5) with the known wake sheet roll-up surface, to get the potentials on the body and potential jumps in the wake.
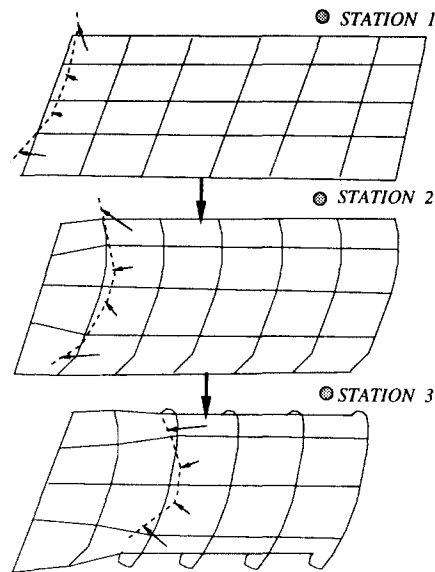
Figure 1. The first iteration of the iteration scheme.

6. Repeat steps 2 to 5 until the geometry of the wake sheet is converged.

In the calculation of the wake sheet roll-up, it usually takes two iterations with given potentials on the body and the potential jumps in the wake. On the other hand, for the construction of the Flow Adapted Grid with wake sheet roll-up, two iterations are usually enough. The computation time for this procedure was 880 sec on DEC Alpha 600 5/266, which is three times as long as the panel method without wake sheet roll-up.

2.3 Determining the tip vortex detachment point

The expanded blade outline curve is found as a cubic B-spline curve. With this outline, the arc length from the hub to the highest radial position (T) along the blade leading edge is found, which is $\widehat{AT}$. When the tip vortex detachment point is assumed to be at T, the wake sheet is not contracted. As a result of this and due to the fact that the wake sheet intersects the blade, the wake alignment procedure diverges as shown at the top of Figure 2.

If the detachment point moves downstream along the trailing edge($\widehat{AS}$ = 1.79), the rolled-up wake at the tip leaves the blade smoothly as is also shown in the same figure. The tip vortex detachment point is determined by moving the tip until the rolled-up wake at the tip leaves the blade smoothly. In addition to requiring smooth detachment at the tip we require that the area where the predicted pressure distribution is singular be minimized. To this moment this process is applied manually. In other words the user has to try different tips until he or she finds which one is *"suitable"*. Usually, $\widehat{AS}$ = 1.15 × $\widehat{AT}$ for a highly skewed propeller, and $\widehat{AS}$ = 1.20 × $\widehat{AT}$ for a propeller with no skew.

2.4 Results

Consider a propeller subject to a spatially uniform flow $V_A(r)$. The flow around the propeller will be analyzed with respect to the propeller fixed coordinate system (x, y, z). If the propeller rotates
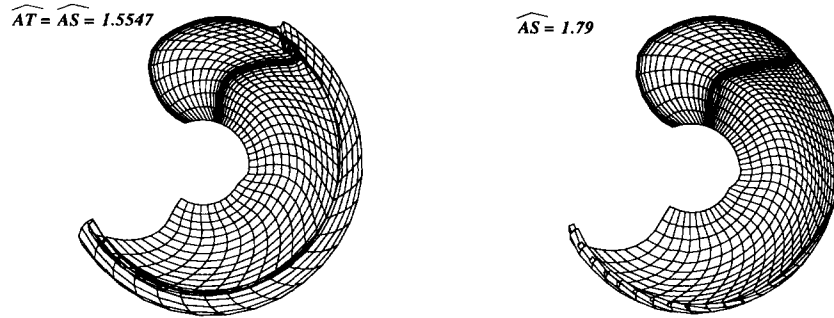
$$\widehat{AT} = \widehat{AS} = 1.5547 \qquad\qquad\qquad \widehat{AS} = 1.79$$

Figure 2. The tip vortex detachment point and wake sheet roll-up.

with angular velocity ω, then the inflow U_{in} at x, relative the propeller is given as
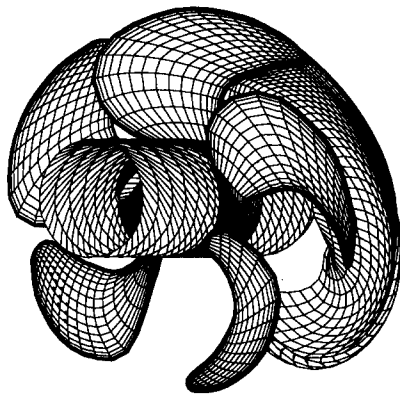
$$U_{in}(x) = V_A(r) - \omega \times x$$

Figure 3. The flow adapted grid on the blades and hub, and 3-D wake sheet surface, as predicted by the present method

For all the computations described in this section, the values of the ultimate wake radius and the tip vortex contraction angle are computed by the method, rather than being given from experimental information. Following the numerical procedure described earlier, the flow adapted grid with the wake sheet roll-up, is applied to the propeller DTMB 4990. The resulting panel arrangement on the blades and hub are shown in Figure 3. This propeller combines a wide tip geometry and a high skew at the tip.

The pressure distribution, predicted from the boundary element method applied on the conventional and the flow adapted grids, are shown in Figures 4. Notice the singular behavior of the pressure at the tip in the case of the conventional grid. In order to compare the tip vortex trajectory with experimental data, the method is applied to propeller DTMB 4119 [Jessup, 1989]. Figure 5 shows the trajectory of the tip vortex along the x-direction. The tip vortex trajectory predicted by the present method is shown to be very close to that measured in the experiment.

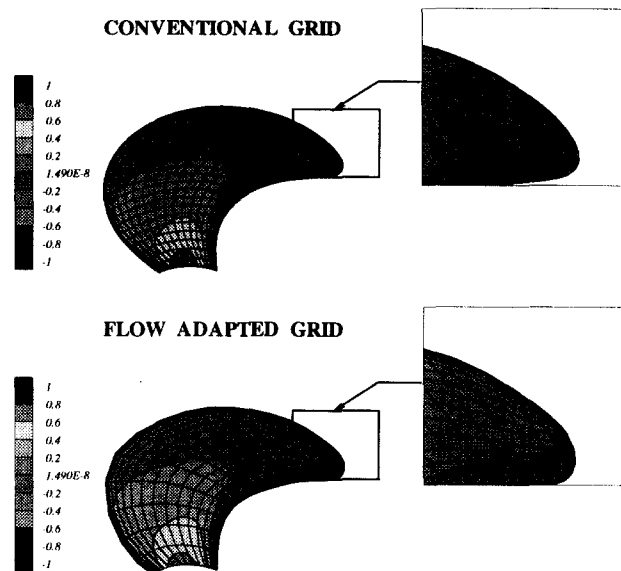CONVENTIONAL GRID

FLOW ADAPTED GRID

Figure 4. Pressure coefficients predicted from a boundary element method applied on the conventional grid(above) and the flow adapted grid (below); propeller 4990, J=1.270.
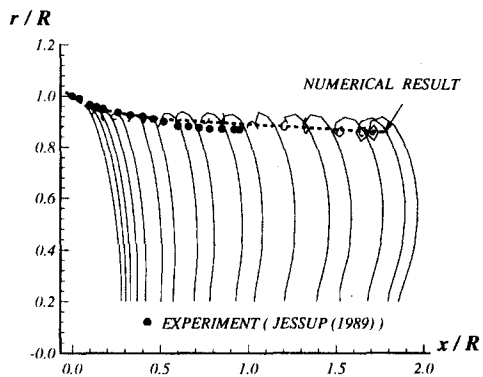

Figure 5. Radial location of the tip vortex for propeller 4119.

3 The flow inside the core

The rolled-up region is modeled as an inviscid core shielded from the outer flow. Deep inside the inviscid core lies the viscous subcore. The cores tend to be slender and have large gradients in the radial direction as compared to the axial direction. As a consequence, the governing equations become parabolic in the axial direction and streamwise diffusion effects are negligible.

An orthogonal curvilinear coordinate system can be established in which the core axis s (also the tip vortex trajectory axis) coincides with one of principal axes of this curvilinear system. The other coordinates (r, θ) are defined in a plane normal to the local tangential vector to s. Then
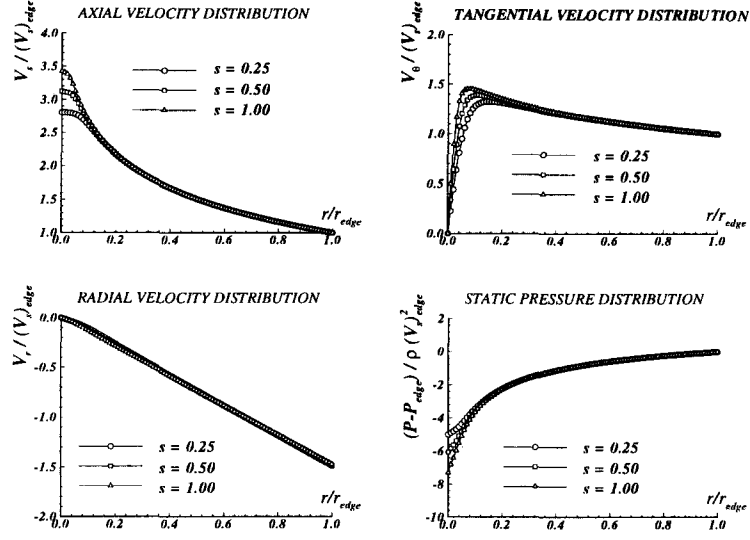
Figure 6. Symmetric velocity and static pressure distribution in the vortex core

the non-dimensionalized Navier-Stokes equations for steady incompressible laminar flow in this coordinate system become ;

$$v_r \frac{\partial v_r}{\partial r} + \frac{v_\theta}{r}\frac{\partial v_r}{\partial \theta} - \frac{v_\theta^2}{r} + v_s\frac{\partial v_r}{\partial s} = -\frac{\partial p}{\partial r}$$

$$+ \frac{1}{Re}\left[\frac{\partial}{\partial r}\left(\frac{1}{r}\frac{\partial}{\partial r}(rv_r)\right) + \frac{1}{r^2}\frac{\partial^2 v_r}{\partial \theta^2} + \frac{\partial^2 v_r}{\partial s^2} - \frac{2}{r^2}\frac{\partial v_\theta}{\partial \theta}\right] \tag{6}$$

$$v_r \frac{\partial v_\theta}{\partial r} + \frac{v_\theta}{r}\frac{\partial v_\theta}{\partial \theta} + \frac{v_r v_\theta}{r} + v_s\frac{\partial v_\theta}{\partial s} = -\frac{1}{r}\frac{\partial p}{\partial \theta}$$

$$+ \frac{1}{Re}\left[\frac{\partial}{\partial r}\left(\frac{1}{r}\frac{\partial}{\partial r}(rv_\theta)\right) + \frac{1}{r^2}\frac{\partial^2 v_\theta}{\partial \theta^2} + \frac{\partial^2 v_\theta}{\partial s^2} + \frac{2}{r^2}\frac{\partial v_r}{\partial \theta}\right] \tag{7}$$

$$v_r \frac{\partial v_s}{\partial r} + \frac{v_\theta}{r}\frac{\partial v_s}{\partial \theta} + v_s\frac{\partial v_s}{\partial s} = -\frac{\partial p}{\partial s}$$

$$+ \frac{1}{Re}\left[\frac{1}{r}\frac{\partial}{\partial r}\left(r\frac{\partial v_s}{\partial r}\right) + \frac{1}{r^2}\frac{\partial^2 v_s}{\partial \theta^2} + \frac{\partial^2 v_s}{\partial s^2}\right] \tag{8}$$

In the r, θ, s coordinate system the flow appears axisymmetric with minor asymmetric variation about the s axis. In addition, from the slender core assumption, two small parameters for the core can be introduced. The governing equations can be reduced to a hierarchy of less complicated equations via a perturbation analysis. Under the perturbation analysis the velocities and pressure
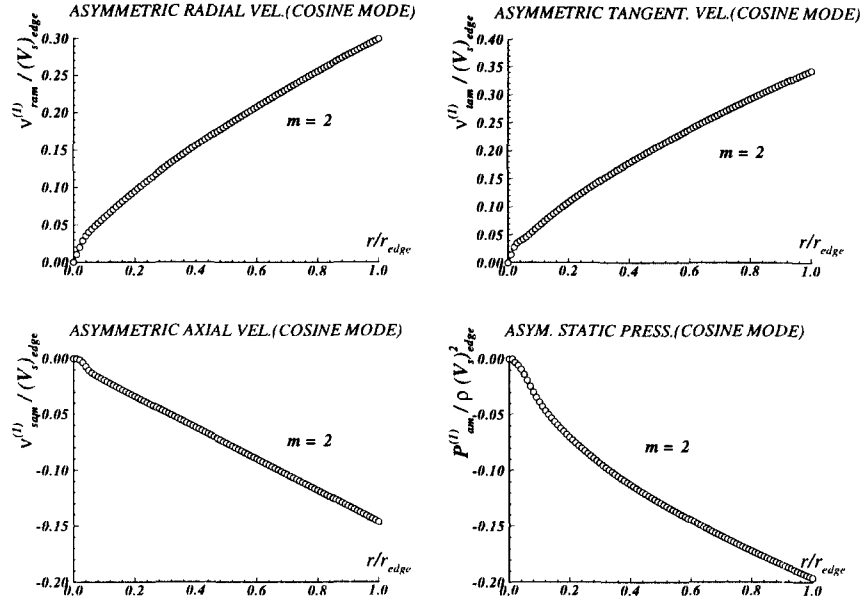
Figure 7. Asymmetric velocity and pressure distribution in the vortex core: cosine modes for m=2.

can be written as

$$v_r = V_r(r,s) + v_r^{(1)}(r,\theta,s) + v_r^{(2)}(r,\theta,s) + \cdots$$

$$v_\theta = V_\theta(r,s) + v_\theta^{(1)}(r,\theta,s) + v_\theta^{(2)}(r,\theta,s) + \cdots$$

$$v_s = V_s(r,s) + v_s^{(1)}(r,\theta,s) + v_s^{(2)}(r,\theta,s) + \cdots$$

$$p = P(r,s) + p^{(1)}(r,\theta,s) + p^{(2)}(r,\theta,s) + \cdots \tag{9}$$

In addition the 1-st order quantities $v_r^{(1)}, v_\theta^{(1)}, v_s^{(1)}, p^{(1)}$ are expressed as Fourier series.

$$v_r^{(1)} = \sum_{m=1}^{\infty} \left(v_{ram}^{(1)} \cos m\theta + v_{rbm}^{(1)} \sin m\theta \right)$$

$$v_\theta^{(1)} = \sum_{m=1}^{\infty} \left(v_{\theta am}^{(1)} \cos m\theta + v_{\theta bm}^{(1)} \sin m\theta \right)$$

$$v_s^{(1)} = \sum_{m=1}^{\infty} \left(v_{sam}^{(1)} \cos m\theta + v_{sbm}^{(1)} \sin m\theta \right)$$

$$p^{(1)} = \sum_{m=1}^{\infty} \left(p_{am}^{(1)} \cos m\theta + p_{bm}^{(1)} \sin m\theta \right) \tag{10}$$

By substituting equations (9), (10) and balancing terms of like order, equations (6),(7),(8) can be written as follows:

27

- 0-th order

$$\frac{V_\theta^2}{r} = \frac{\partial P}{\partial r}$$

$$\frac{V_r}{r}\frac{\partial}{\partial r}(rV_\theta) + V_s\frac{\partial V_\theta}{\partial s} = \frac{1}{Re}\frac{\partial}{\partial r}\left(\frac{\partial V_\theta}{\partial r} + \frac{V_\theta}{r}\right)$$

$$V_r\frac{\partial V_s}{\partial r} + V_s\frac{\partial V_s}{\partial s} = -\frac{\partial P}{\partial s} + \frac{1}{Re}\left(\frac{\partial^2 V_s}{\partial r^2} + \frac{1}{r}\frac{\partial V_s}{\partial r}\right)$$

$$\frac{1}{r}\frac{\partial}{\partial r}(rV_r) + \frac{\partial V_s}{\partial s} = 0 \tag{11}$$

The 0-th order equations govern slender axisymmetric flow. They are the parabolised Navier-Stokes equations. This problem can be numerically solved [Hall, 1965]. The scheme does not require the core to be conical and is therefore suitable for studies of non-delta wings such as propeller blades.

Preliminary computations are made for a vortex core whose radius r_c grows linearly with s so that $r_{edge} = 0.04$ at $s = 1$ with $Re = 10^6$. The conical boundary conditions are assumed from $s = 1/$Number of panel to $s = 1$: $V_s = V_\theta = 1.0$. P at the core edge is set to constant because only the differentials of P is needed. An uniform axial velocity and a solid body rotation are taken as initial conditions. The results from this computation are shown in Figure 6. In the figure, the axial velocity in the core reaches a peak of 3.5 times the edge velocity. V_r is very small because of slenderness assumption.

- 1-st order

$$L_r\left[v_{ram}^{(1)}\right] = 0$$

$$L_r\left[v_{rbm}^{(1)}\right] = 0$$

$$\frac{v_{ram}^{(1)}}{r}\frac{\partial}{\partial r}(rV_\theta) + \frac{mV_\theta}{r}v_{\theta bm}^{(1)} + m\frac{p_{bm}^{(1)}}{r} = 0$$

$$\frac{\partial V_s}{\partial r}v_{ram}^{(1)} + m\frac{V_\theta}{r}v_{sbm}^{(1)} = 0$$

$$\frac{\partial v_{ram}^{(1)}}{\partial r} + \frac{v_{ram}^{(1)}}{r} + \frac{mv_{\theta bm}^{(1)}}{r} = 0$$

$$\frac{v_{rbm}^{(1)}}{r}\frac{\partial}{\partial r}(rV_\theta) - \frac{mV_\theta}{r}v_{\theta am}^{(1)} - m\frac{p_{am}^{(1)}}{r} = 0$$

$$\frac{\partial V_s}{\partial r}v_{rbm}^{(1)} - m\frac{V_\theta}{r}v_{sam}^{(1)} = 0$$

$$\frac{\partial v_{rbm}^{(1)}}{\partial r} + \frac{v_{rbm}^{(1)}}{r} - \frac{mv_{\theta am}^{(1)}}{r} = 0$$

$$L_r = \frac{\partial^2}{\partial r^2} + \frac{3}{r}\frac{\partial}{\partial r} - \left(\frac{V_\theta'' + V_\theta'/r}{V_\theta} + \frac{m^2 - 2}{r^2}\right) \tag{12}$$
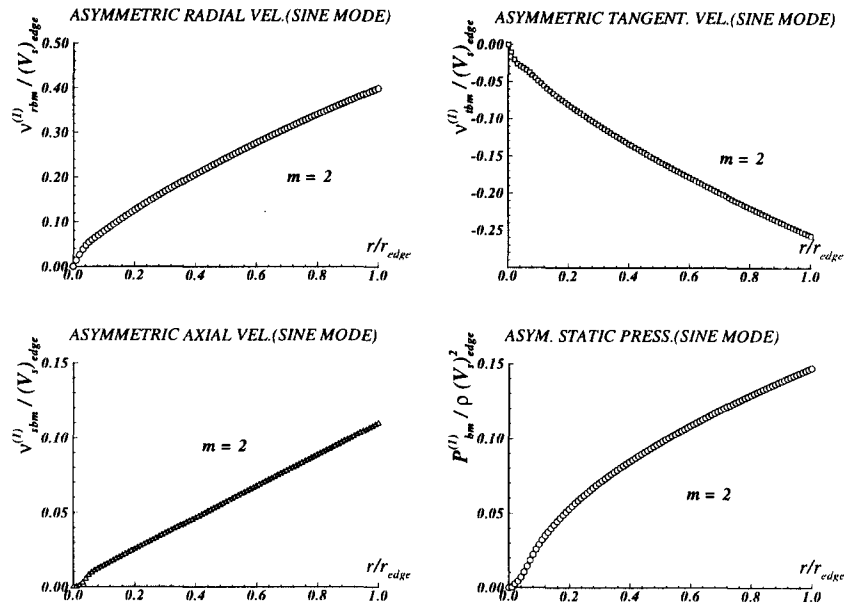
28

Figure 8. Asymmetric velocity and pressure distribution in the vortex core: sine modes for m=2.

The asymmetric equations for the 1-st order can also be solved numerically [Lee, 1991]. The boundary values $v^{(1)}_{r_{ame}}$ and $v^{(1)}_{r_{bme}}$ are set to 0.3, 0.4, respectively for $m = 2$. Asymmetric solutions in the form of cosine and sine modes are shown in Figure 7, 8 for radial, tangential, axial velocities and pressure, respectively. In the figure, all asymmetric values are zero at $r = 0$ and the values agree exactly with those from Lee [Lee, 1991]. Since two numerical results from the present method and the Lee's method are exactly the same, the result from the present method is only shown in Figure 7, 8.

4 Conclusions

A robust and efficient three-dimensional numerical method has developed for accurately predicting the pressure in the vicinity of the blade tip.

- The method is applied to propeller geometries and the predicted tip vortex trajectories are shown to agree very well to those reported in experiments.

- the method also improves the predicted pressures at the tip.

In addition, the viscous method for the analysis of the flow inside the tip vortex core is suggested.

- The velocities from the method shows good agreement with other numerical method.

- In order to calculate the flow inside the viscous core, the velocities and pressure at the edge of the core from the proposed potential method, should be matched along the core edge.

References

1. McCormick, B.W., 1962, On Vortex Produced By a Vortex Trailing From a Lifting Surface, Journal of Basic Engineering, September, pp. 369–379.

2. Fruman, D., Dugué, C., Pauchet, A., Cerruti, P. and Briançon-Marjolet, L., 1992, Tip Vortex Roll-Up and Cavitation, Proc. Nineteenth Symposium on Naval Hydrodynamics, pp. 633–654, Seoul ,Korea.

3. Dupont, P. and Cerrutti, P., 1991, Comparison between Tip Vortex Development Calculations and Measurements on an Elliptic Planform, Third European FIDAP Users Group Meeting, September.

4. Eça, L., Falcão de Campos, J. and Hoekstra, M., 1994, Prediction of Incompressible Tip Vortex Flow, Proc. Twentieth Symposium on Naval Hydrodynamics, Santa Barbara, California.

5. Stern, F., Zhang, B., Chen, B., Kim, H. and Jessup, S., 1994, Computation of Viscous Marine Propulsor Blade and Wake Flow, Proc. Twentieth Symposium on Naval Hydrodynamics, Santa Barbara, California.

6. Pyo, S., 1995, Numerical Modeling of Propeller Tip Flows with Wake Sheet Roll-Up in Three Dimensions, Ph.D. thesis, M.I.T., Department of Ocean Engineering.

7. Hsin, C-Y., 1990, Development and Analysis of Panel Method for Propellers in Unsteady Flow, Ph.D. thesis, M.I.T., Department of Ocean Engineering.

8. Jessup, S.D., 1989, An Experimental Investigation of Viscous Aspects of Propeller Blade Flow, Ph.D. thesis, The Catholic University of America.

9. Maniar,H. D., 1995, A Three Dimensional Higher Order Panel Method, Ph.D. thesis, M.I.T., Department of Ocean Engineering.

10. Lee, J.-T., 1987, A Potential Based Panel Method for The Analysis of Marine Propellers in Steady Flow, Ph.D. thesis, M.I.T., Department of Ocean Engineering.

11. Arndt, R.E.A., Arakeri, V. H., and Higuchi, H., 1991, Some observations of tip vortex cavitation, JOURNAL OF FLUID MECHANICS, Vol 229, pp. 269–289.

12. Hall, M.G., 1965, A Numerical Method for Solving the Equations for a Vortex Core, Aerospace Research Council Report & Memorenda, No.3467.

13. Lee, N., 1991, Evolution and Structure of Leading Edge Vortices over Slender Wings, Ph.D. thesis, M.I.T., Department of Aero. and Astro.